Electronic Supplementary Material (ESI) for Dalton Transactions.


# Supporting Information

## Synergistic Effect of the Composite Films Formed by Zeolitic Imidazolate Framework 8 (ZIF-8) and Porous Nickel Films for Enhanced Amperometric Sensing of Hydrazine

*Erbin Shi, Huiming Lin, Qian Wang, Feng Zhang*, Shaoxuan Shi, Tingting Zhang, Xin Li, Hao Niu and Fengyu Qu**

College of Chemistry and Chemical Engineering, Harbin Normal University, Harbin, Heilongjiang 150025 (P. R. China)

## The hydrazine adsorption on the ZIF-8 NPs, Ni porous film and ZIF-composite film

### Adsorption procedure

The stock solution (1000 mg/L) of hydrazine was prepared by diluting 44.5 μL of $N_2H_4.H_2O$ (wt 85%) in double distilled water. Hydrazine solution with different initial concentrations ($C_0$) was obtained by diluting the stock solutions with doubled distilled water. The adsorption of the hydrazine by the different materials was performed by mixing the dried samples (10 mg) and hydrazine solutions with different initial concentrations ($C_0$) (20 mL). The mixtures were left in a stirred operating at room temperature for 12 h to reach equilibrium. After reaching adsorption equilibrium, the supernatant and the films (the Ni porous film and the ZIF-composite film) were separated by decantation. The residual solution were separated from ZIF-8 powders by centrifugation at 8,000 rpm for 10 min. The concentrations of hydrazine in solutions were measured by UV-visible spectrophotometer.

### Analytical procedure of bromate concentrations

Calibration curve of the hydrazine was obtained by following process: in a brown volumetric flask (25.00 mL), a certain amount hydrazine was added to 5 mL of p-dimethylaminobenzaldehyde (DMAB) solution (4 g DMAB dissolved in a flasks containing 200 mL 95 % ethanol and 20 mL 12 M hydrochloric acid), and then diluted with hydrochloric acid solution (0.12 M), and mixed. After 20 min, the yellow colored complex formed from DMAB and hydrazine in acidic solutions was final recorded at 458 nm using the Ultraviolet-spectrophotometer (UV 2600; Shimadzu, Japan) (**Figure S14a**).

After removing the powders and film materials (the ZIF-8 NPs, the Ni porous film and the ZIF-composite film), the concentrations of hydrazine remaining in supernatant solutions were measured by the procedure mentioned above. The amount of hydrazine was calculated by using the calibration curve of hydrazine solutions (**Figure S14b**).

## BET equation:

$$V = \frac{V_m CP}{(P_0 - P)\left[1 + (c-1)(P/P_0)\right]} \text{.....S1}$$

where $V$ is the volume of nitrogen adsorbed per gram of MOF at STP, $V_m$ is the monolayer capacity, and $C$ is related to the heat of adsorption.

The equation can be changed in the form:

$$\frac{P/P_0}{V(1-P/P_0)} = \frac{(C-1)P/P_0}{V_m C} + \frac{1}{V_m C} \text{.....S2}$$

A plot of the $\frac{P/P_0}{V(1-P/P_0)}$ *vs.* $P/P_0$ for ZIF-8 is shown below for the isotherm given in Figure S8. Notice that the line is fit to the low pressure isotherm data, which is well below the standard BET range of $0.05 < P/P_0 < 0.3$

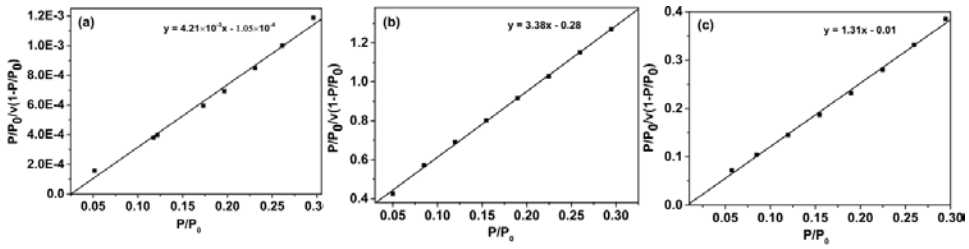


Plots of the $\frac{P/P_0}{V(1-P/P_0)}$ *vs.* $P/P_0$ on the ZIF-8 (a), Ni porous film (b) and (c) ZIF-composite film at the standard BET range of $0.05 < P/P_0 < 0.3$.

The slope and y-intercept of the line yield $C = 40.95$ and $(V_m)_{(STP)} = 231.73$ $cm^3g^{-1}$.

$$S_{BET} = N_m V_m \sigma_0 N_A \text{.....S3}$$

where $(N_m)_{STP}$ is the molar density of nitrogen at standard temperature and pressure (44.6 mol $m^{-3}$), $\sigma_0$ is the effective cross-sectional area of nitrogen at liquid state ($1.62 \times 10^{-19}$ $m^2$), and $N_A$ is Avogadro's number ($6.02 \times 10^{23}$ $mol^{-1}$).

The BET surface area was calculated to 1007.93 $m^2$ $g^{-1}$. Also, the Ni porous film and the ZIF-composite film were 1.19 $m^2$ $g^{-1}$and 3.28 $m^2$ $g^{-1}$, respectively, using the same method mentioned above.

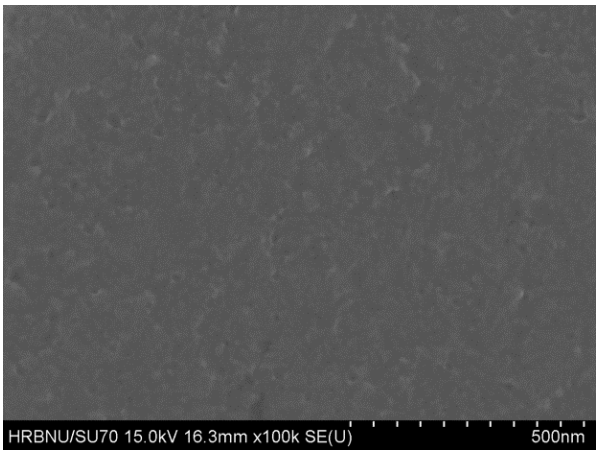


**Figure S1** SEM image of the Ni/Cu alloy film.

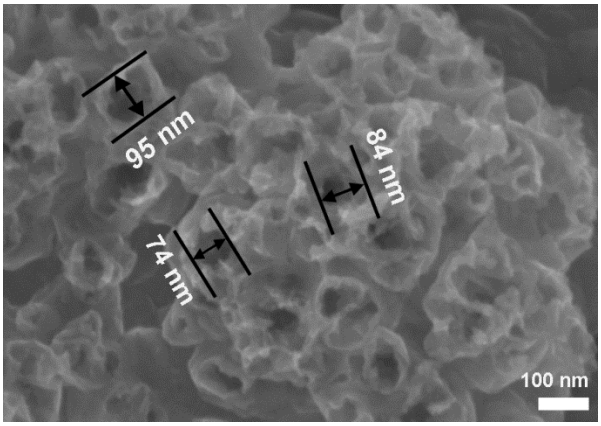


**Figure S2** The enlarge SEM image of the Ni porous film.

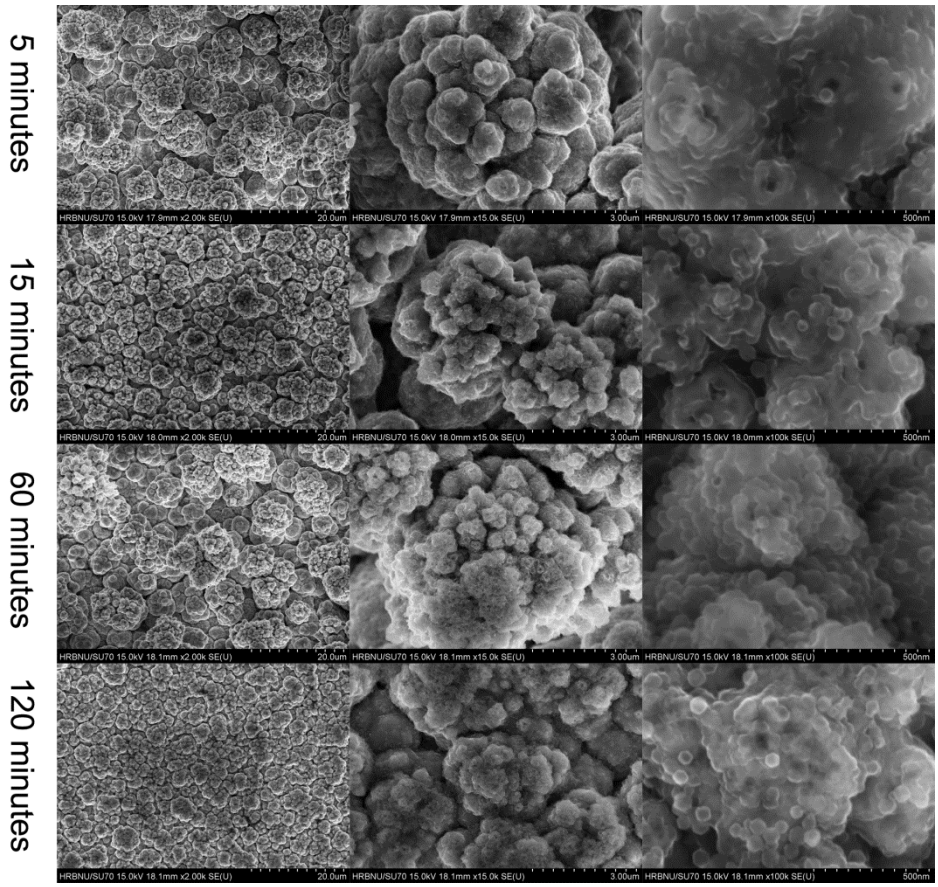


**Figure S3** SEM images of ZIF-Ni composite films obtained by *in-situ* deposition of ZIF-8 on the Ni porous films for different deposition time of 5, 15, 60 and 120 minutes, respectively.

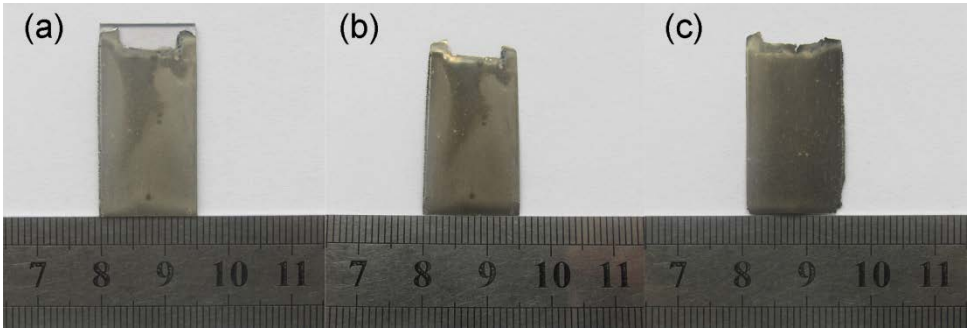


**Figure S4** The photo images of the Ni porous film on ITO (a), the Ni porous film exfoliated from ITO (b), the ZIF-Ni composite film for the deposition time of 30 min.

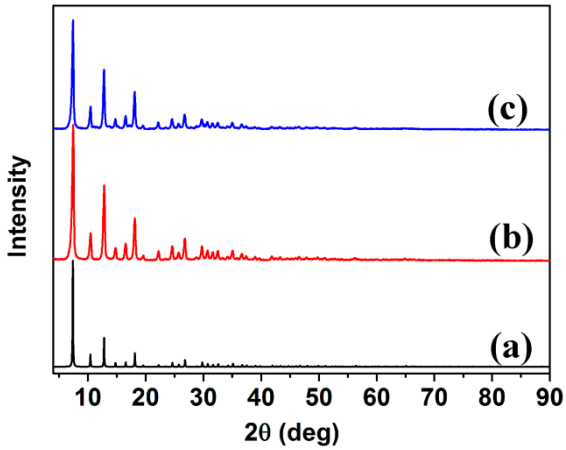


**Figure S5** XRD patterns of the simulated ZIF-8 (a), the powders collected by the aqueous solution of ZIF-Ni composite films for the deposition of 30 min (b), and the sample (b) after immersion in 0.1 M NaOH at room temperature for 24 hr.

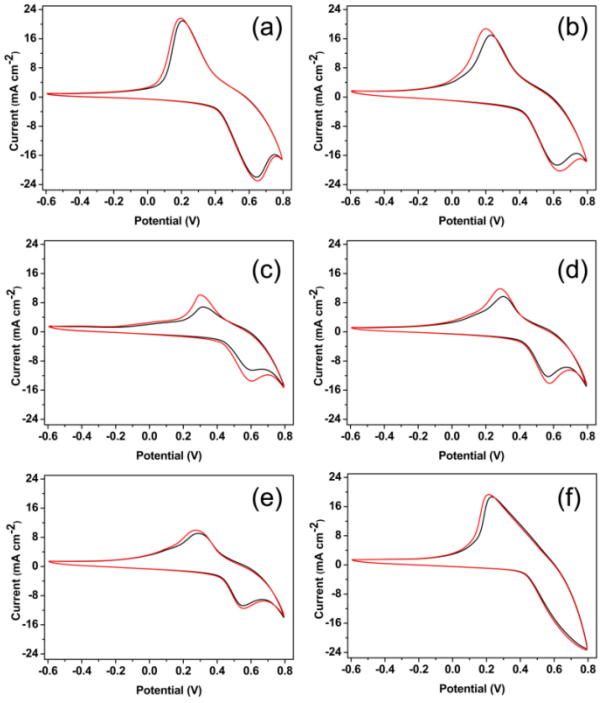


**Figure S6** CV responses of the ZIF-Ni composite films obtained by *in-situ* deposition of ZIF-8 on the Ni porous films for different deposition time of 5 min (a), 15 min (b), 30 min (c), 60 min (d), 120 min (e) and 240 min (f) with absence (black) and presence (red) of 0.2 mM hydrazine in NaOH solution (0.1 M) at a scan rate of 50 mV $s^{-1}$.

11/04/201617:57:45

| | Ni 231.604 |
|---|---|
| | mg/L |
| Ni*20 | 17.06 ×20 = 341.2 |
| | **Zn 213.857** |
| | mg/L |
| Zn | 10.19 |

**Figure S7** The amount of nickel ions and zinc ions obtained by the inductively coupled plasma-emission spectroscopy (ICP-ES). The composite film was digested with sonication in HCl solution (2M), and by analyzing the ICP data, it is calculated that there are approximately 1.5 wt.% ZIF-8 in the ZIF-Ni composite film.

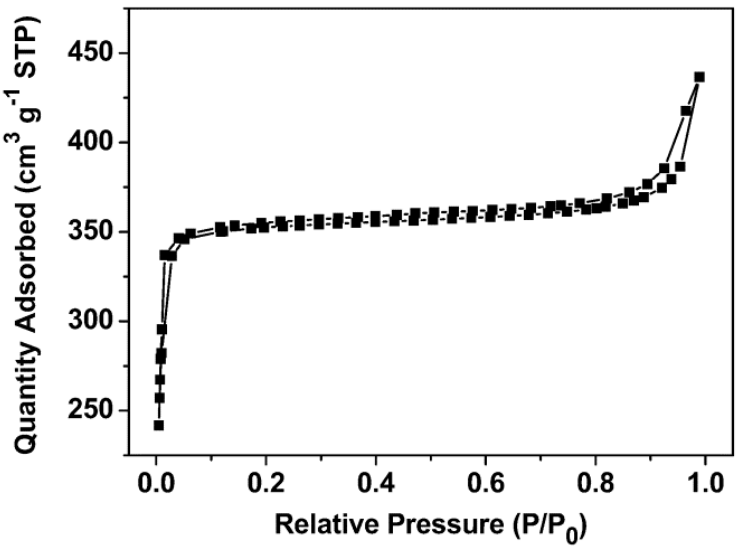


**Figure S**8 $N_2$ adsorption-desorption isotherm of ZIF-8 collected by the aqueous of the ZIF-Ni composite film for 30 min.

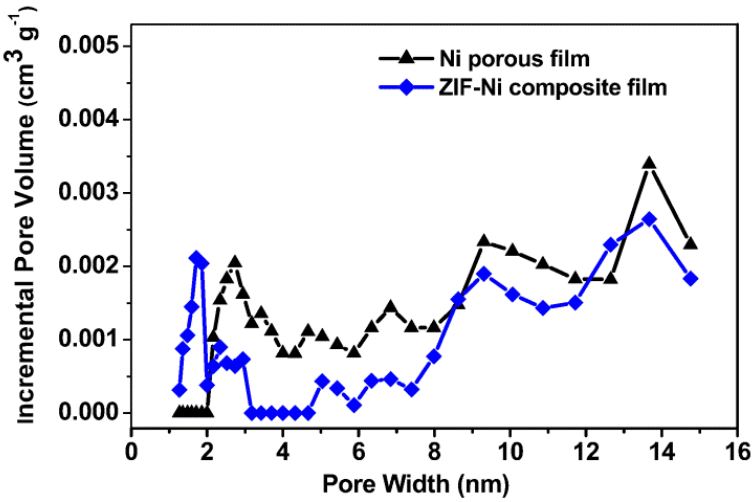


**Figure S**9 The pore size distributions of the Ni porous film and ZIF-Ni composite film (30 min) adopted by the nonlocal density functional theory (NLDFT).

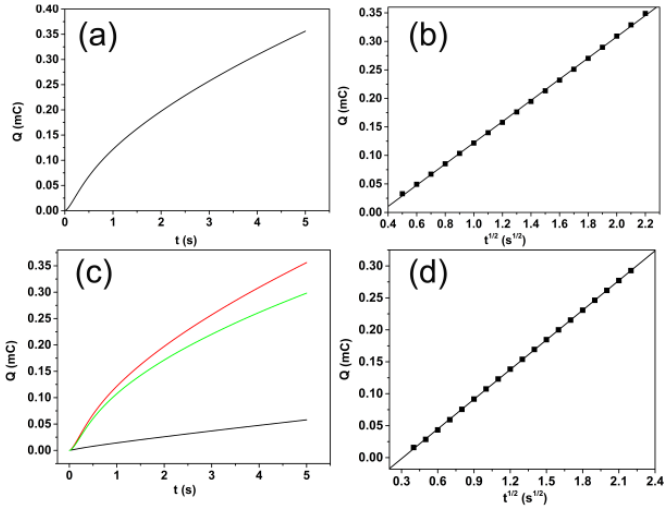


**Figure S**10 (a) Chronocoulometry response and (b) the corresponding Q-$t^{1/2}$ curve of the GCE in the $K_3[Fe(CN)_6]$ solution containing 0.1 M KCl. (c) Chronocoulometry response of the GCE in the absence (black) and the presence (red) of 0.2 mM hydrazine at the 0.1 M NaOH solution and the corresponding Q-t curve after the background subtracted (green). (d) The Q-$t^{1/2}$ plot on the composite film after the background subtracted.

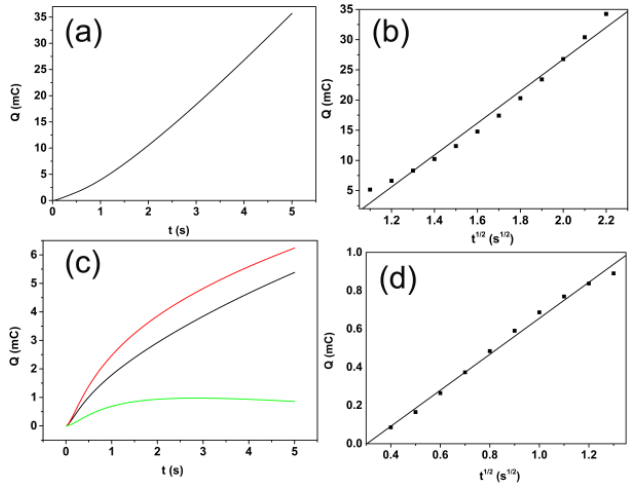


**Figure S**11 (a) Chronocoulometry response and (b) the corresponding Q-$t^{1/2}$ curve of the Ni porous film in the $K_3[Fe(CN)_6]$ solution containing 0.1 M KCl. (c) Chronocoulometry response of the Ni porous film in the absence (black) and the presence (red) of 0.2 mM hydrazine at the 0.1 M NaOH solution and the corresponding Q-t curve after the background subtracted (green). (d) The Q-$t^{1/2}$ plot on the composite film after the background subtracted.

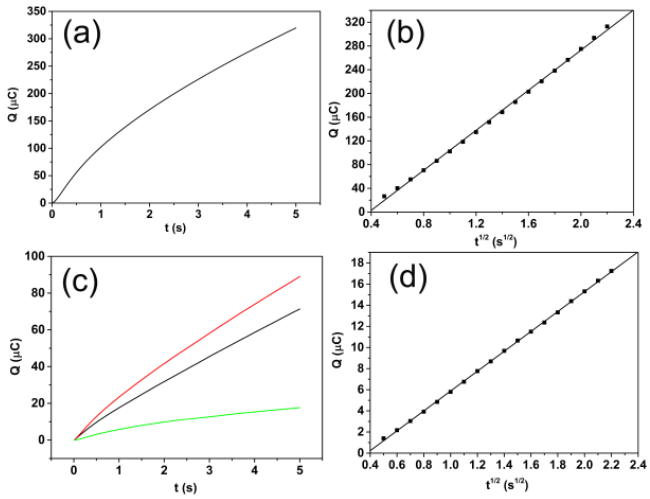


**Figure S**12 (a) Chronocoulometry response and (b) the corresponding Q-$t^{1/2}$ curve of the ZIF-8 NP/GCE in the $K_3[Fe(CN)_6]$ solution containing 0.1 M KCl. (c) Chronocoulometry response of the ZIF-8 NP/GCE in the absence (black) and the presence (red) of 0.2 mM hydrazine at the 0.1 M NaOH solution and the corresponding Q-t curve after the background subtracted (green). (d) The Q-$t^{1/2}$ plot on the composite film after the background subtracted.

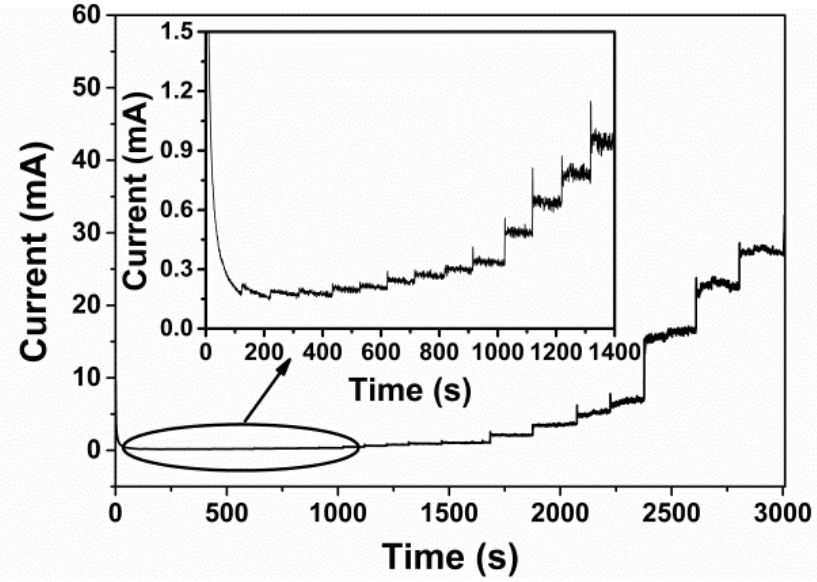


**Figure S13** Amperometric response of the ZIF-Ni composite film at an applied potential of 0.55 V upon the successive addition of hydrazine aliquots into a stirred NaOH solution (0.1 M); Insert: Amplified Amperometric response of the composite film during 800 s.

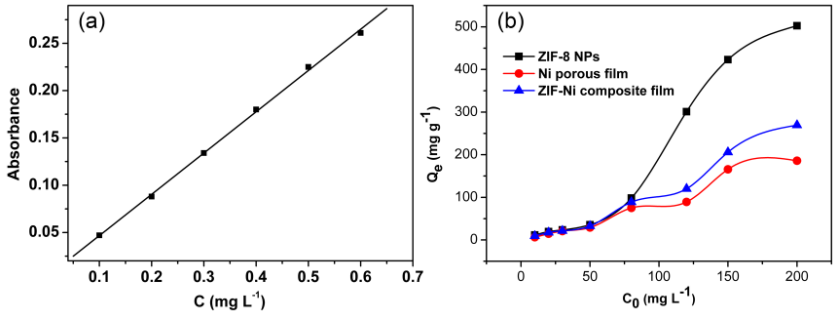


**Figure S14** (a) Standard curve of UV absorbance of the hydrazine solutions in the function of concentrations in water. (b) Adsorption isotherm for hydrazine on the ZIF-8 NPs (black curve), the Ni porous film (red curve) and the ZIF-composite film (blue curve).

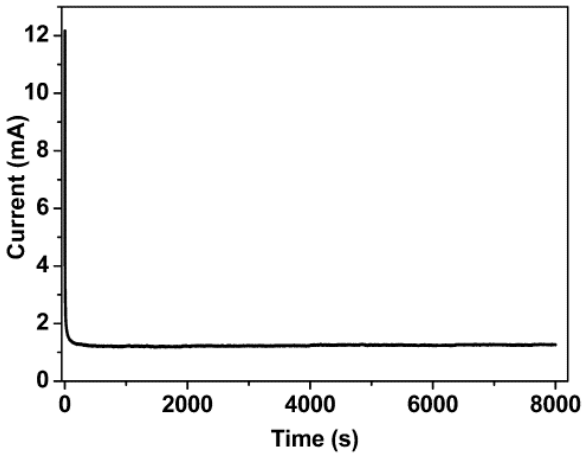


**Figure S15** Stability of the chronoamperometry response to 0.2 mM hydrazine during 8000 s.

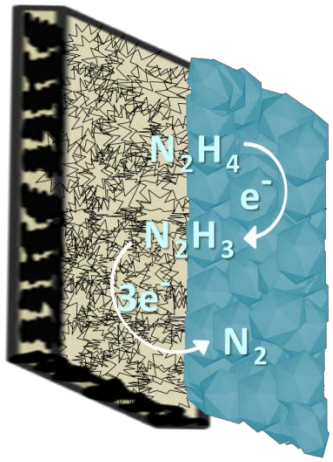


**Scheme S1** The electrocatalytic process of hydrazine for the composite film.

**Table S1** The effective area and adsorption capacity for hydrazine of the work electrodes.

| Work electrodes | Effective area ($cm^2$) | Adsorption capacity (mol $cm^{-2}$) |
|---|---|---|
| GCE | 0.62 | $2.0 \times 10^{-10}$ |
| ZIF-8/GCE | 0.58 | $1.5 \times 10^{-11}$ |
| Ni porous film | 88.0 | $8.4 \times 10^{-12}$ |
| ZIF-Ni composite film | 13.3 | $2.3 \times 10^{-10}$ |

*GCE = glass carbon electrode

**Table S2** Comparison of different modified electrodes and different methods for the hydrazine detection.

| Electrode | Method | Detection limit (μM) | Sensitivity ($\mu A \cdot mM^{-1}$) | Linear range (μM) | Refs |
|---|---|---|---|---|---|
| Ni(II)-BA-MWCNT-PE | AP | 0.8 | 69.9 | 2.5–200 | 1 |
| PEG-coated ZnS | AP | 1.073 | 89.3 | 1–3,000 | 2 |
| Graphene nanoflakes | CA | 0.3 | 28 | 0.5–7.5 | 3 |
| ZnO nanoflower | AP | 0.18 | 246.9 | 0.6–250 | 4 |
| HTP-MWCNT-CPE | DPV | 0.13 | 12.6 | 1.0–6,000 | 5 |
| PVP-AgNCs/GCE | AP | 1.1 | - | 5–460 | 6 |
| Hematoxylin MWCNTs | AP | 0.68 | 20.8 | 2.0–122.8 | 7 |
| Rhodium | AP | 3 | 26.3 | 5–10,000 | 8 |
| Au/PPy/GCE | DPV | 0.2 | 126 | 1–500 | 9 |
| GNPs/Ch/GCE | LSV | 0.1 | 89.1<br>84.3 | 0.5–500<br>500–9,300 | 10 |
| CoOOH nanosheet | AP | 20 | 122 | 0–1200 | 11 |
| Ag/ZIF-8/CPE | AP | 1.57 | - | 6-5,000 | 12 |
| ZIF-Ni composite film | AP | 0.02 | 805.5 | 2.5-28,000 | Present work |


1. L. Zheng and J.-f. Song, *Talanta*, 2009, 79, 319-326.
2. S. K. Mehta and A. Umar, *Talanta*, 2011, 85, 2411-2416.
3. S. Mutyala and J. Mathiyarasu, *Sensors and Actuators B: Chemical*, 2015, 210, 692-699.
4. B. Fang, C. Zhang, W. Zhang and G. Wang, *Electrochimica acta*, 2009, 55, 178-182.
5. H. R. Zare, M. R. Shishehbore, D. Nematollahi and M. S. Tehrani, *Sensors and Actuators B: Chemical*, 2010, 151, 153-161.
6. Y. Wang, X. Yang, J. Bai, X. Jiang and G. Fan, *Biosensors and Bioelectronics*, 2013, 43, 180-185.
7. H. R. Zare and N. Nasirizadeh, *Electrochimica acta*, 2007, 52, 4153-4160.
8. J. Pingarron, I. O. Hernández, A. González-Cortés and P. Yanez-Sedeno, *Analytica chimica acta*, 2001, 439, 281-290.
9. J. Li and X. Lin, *Sensors and Actuators B: Chemical*, 2007, 126, 527-535.
10. J. Li, H. Xie and L. Chen, *Sensors and Actuators B: Chemical*, 2011, 153, 239-245.
11. K. K. Lee, P. Y. Loh, C. H. Sow and W. S. Chin, *Biosensors and Bioelectronics*, 2013, 39, 255-260.
12. A. Samadi-Maybodi, S. Ghasemi and H. Ghaffari-Rad, *Sensors and Actuators B: Chemical*, 2015, 220, 627-633.